



**HAL**  
open science

## Fluorescent chitosan-based nanohydrogels and encapsulation of gadolinium MRI contrast agent for magneto-optical imaging

Juliette Moreau, Maité Callewaert, Volodymyr Malytskyi, Céline Henoumont, Sorina Voicu, Miruna Stan, Michael Molinari, Cyril Cadiou, Sophie Laurent, Françoise Chuburu

### ► To cite this version:

Juliette Moreau, Maité Callewaert, Volodymyr Malytskyi, Céline Henoumont, Sorina Voicu, et al.. Fluorescent chitosan-based nanohydrogels and encapsulation of gadolinium MRI contrast agent for magneto-optical imaging. *Carbohydrate Polymer Technologies and Applications*, 2021, 2, pp.100104. 10.1016/j.carpta.2021.100104 . hal-03523383

**HAL Id: hal-03523383**

**<https://hal.univ-reims.fr/hal-03523383v1>**

Submitted on 2 Aug 2023

**HAL** is a multi-disciplinary open access archive for the deposit and dissemination of scientific research documents, whether they are published or not. The documents may come from teaching and research institutions in France or abroad, or from public or private research centers.

L'archive ouverte pluridisciplinaire **HAL**, est destinée au dépôt et à la diffusion de documents scientifiques de niveau recherche, publiés ou non, émanant des établissements d'enseignement et de recherche français ou étrangers, des laboratoires publics ou privés.



Distributed under a Creative Commons Attribution - NonCommercial 4.0 International License

1 **Fluorescent chitosan-based nanohydrogels and encapsulation of gadolinium MRI**  
2 **contrast agent for magneto-optical imaging**

3 *Juliette Moreau,<sup>a\*</sup> Maité Callewaert,<sup>a\*</sup> Volodymyr Malytskyi,<sup>a</sup> Céline Henoumont,<sup>b</sup> Sorina N.*  
4 *Voicu,<sup>c,d</sup> Miruna S. Stan,<sup>c</sup> Michael Molinari,<sup>e</sup> Cyril Cadiou,<sup>a</sup> Sophie Laurent,<sup>b,f</sup> Françoise*  
5 *Chuburu<sup>a\*</sup>*

6 <sup>a</sup> Institut de Chimie Moléculaire de Reims, CNRS UMR 7312, University of Reims  
7 Champagne-Ardenne URCA, 51685 Reims Cedex 2, France.

8 <sup>b</sup> NMR and Molecular Imaging Laboratory, University of Mons, UMons, B-7000  
9 Mons, Belgium.

10 <sup>c</sup> Faculty of Biology, Department of Biochemistry and Molecular Biology, University  
11 of Bucharest, Bucharest, Romania.

12 <sup>d</sup> Faculty of Pharmacy, Department of Pharmacy, Titu Maiorescu University,  
13 Bucharest, Romania.

14 <sup>e</sup> CBMN CNRS UMR 5248, University of Bordeaux, INP Bordeaux, 33600, Pessac,  
15 France

16 <sup>f</sup> Center for Microscopy and Molecular Imaging, Rue Adrienne Bolland 8, B-6041  
17 Charleroi, Belgium.

18

19 **Corresponding Authors** : \*juliette.moreau@univ-reims.fr, \* maite.callewaert@univ-  
20 reims.fr, \* francoise.chuburu@univ-reims.fr

21 **Author Contributions**

22 Juliette Moreau\* (Polymer syntheses, fluorescent nanogel characterizations – writing original  
23 draft), Maite Callewaert\* (Nanogel syntheses, characterizations – writing original draft),  
24 Volodymyr Malytskyi (Polymer syntheses), Céline Henoumont (DOSY and relaxometry  
25 experiments – writing original draft), Sorina N Voicu (Biological assays – writing original  
26 draft), Miruna S. Stan (Biological assays), Michael Molinari (AFM measurements supervision  
27 – writing), Cyril Cadiou (Polymer and fluorescent nanogels characterizations supervision -  
28 Reviewing and editing), Sophie Laurent (NMR supervision of the relaxometry part -  
29 reviewing), Françoise Chuburu\* (Conceptualization, writing – reviewing and editing).

30 The manuscript was written through contributions of all authors. All authors have given  
31 approval to the final version of the manuscript.

## 1 **Highlights:**

- 2 • Control of fluorophores (rhodamine and fluorescein) grafting onto chitosan backbone  
3 by a combination of DOSY and fluorescence analyses.
- 4 • Fluorescent nanohydrogel syntheses by ionotropic gelation between grafted chitosans  
5 and hyaluronic acid.
- 6 • The encapsulation of gadolinium chelate in these fluorescent nanohydrogels  
7 considerably improves the detection sensitivity and thus the contrast in MRI imaging,
- 8 • These fully biocompatible magneto-optical nanohydrogels behave as hypersensitive  
9 MRI probes in  $T_1$ - and  $T_2$ - modes while emitting a green or red light in optical  
10 imaging.

## 11 **Abstract**

12 In the field of medical imaging, multimodal nanoparticles combining complementary imaging  
13 modalities can give rise to new forms of imaging techniques that are able to make diagnosis  
14 more precise and confident. In this context, resolution and sensitivity have often to be  
15 gathered into a single imaging probe, by combination of MRI and optical imaging for  
16 instance. Gadolinium chelate (Gd-CAs) loaded nanohydrogels, obtained from chitosan (CS)  
17 and hyaluronic acid (HA) matrix, have shown their efficiency to greatly improve MRI  
18 contrast ( $r_1 \geq 80 \text{ mM}^{-1} \text{ s}^{-1}$ ). In this study, nanohydrogels were made intrinsically fluorescent  
19 by chitosan pre-functionalization and a series of fluorescent chitosans were obtained by  
20 covalent grafting of rhodamine (Rhod:  $6.3\mu\text{M}$ ) or fluorescein (Fluo:  $7.3\mu\text{M}$ ) tags. By  
21 combining DOSY and fluorescence data, fluorescent chitosans (CS-Rhod and CS-Fluo) with a  
22 low degree of substitution were then selected and used to encapsulate high gadolinium  
23 loadings to obtain efficient magneto-optical nanohydrogels.

24

## 25 **Introduction**

26 Because of its excellent resolution and the absence of patient exposition to ionizing  
27 radiations, MRI plays a central role in the arsenal of imaging techniques available to  
28 radiologists. This technique is recognized for its excellent resolution but suffers from a lack of  
29 sensitivity and information obtained from a simple unenhanced MR image is often not  
30 sufficient to highlight the areas of interest in tissues. Usually, this drawback is compensated  
31 by the injection of paramagnetic substances, in practice gadolinium chelates GdCAs (such as  
32 gadoteric acid also known as DOTAREM®) at high concentration  $> 0.1 \text{ mmol mL}^{-1}$ , whose

1 role is to selectively highlight abnormal tissues by shortening the longitudinal relaxation times  
2 of water protons in these tissues (Merbach, Helm & Toth, 2013). Until recently, GdCAs were  
3 considered as safe but since the incidence of nephrogenic systemic fibrosis (NSF disease) in  
4 patients with unpaired renal function (Rogosnitzky & Branch, 2016) and the observation of  
5 MRI brain abnormalities, even with patients with normal renal function (Kanda et al., 2016),  
6 the problem is now quite different. Elemental analyses of tissues collected after autopsy of  
7 animal models have shown that these manifestations are correlated to *in vivo* Gd  
8 demetallation, favored by the lack of chemical inertia of certain GdCAs (of linear structure,  
9 that have been since withdrawn from the market) (Gianolio et al., 2017). However, there is  
10 currently no clinically available alternative to injecting GdCA during MRI examinations,  
11 when it is necessary (Gupta et al., 2020). The alternative is then needed to improve the  
12 efficacy of low-risk GdCA to enhance the MRI signal. It is also important to keep in mind  
13 that even if MRI provides images with an excellent resolution, it suffers from low sensitivity  
14 detection.

15 A solution is to take advantage of nanoparticle strategy, not only to boost the intrinsic efficacy  
16 of GdCAs (defined by their relaxivity  $r_1$  in  $\text{mM}^{-1} \text{s}^{-1}$ ) and to convert them into hypersensitive  
17 MRI probes, but also to add an optical imaging modality by introduction of fluorophores in  
18 the nanoassembly. We have demonstrated that the confinement of a low-risk GdCA such as  
19 HGdDOTA (Gadolinium(III)-1.4.7.10-Tetraazacyclododecane-1.4.7.10-tetraacetate, which is  
20 the active substance of DOTAREM®) into a nanogel (NG) matrix constituted with  
21 polysaccharide biopolymers such as chitosan CS and hyaluronic acid HA (Courant et al.,  
22 2012; Callewaert et al., 2014) can provide an interesting alternative to greatly increase the  
23 MRI efficacy of GdCAs. Not only do they have the advantage over types of nanogels (Lux et  
24 al., 2013; Soleimani et al., 2013) to overcome the sensitivity disadvantage of Gd contrast  
25 agents (Washner et al., 2019) but they are also biocompatible with a low toxicity which is of  
26 particular interest for biomedical applications.

27 Nanogels are water-rich nanoparticles, which is essential to exalt the MRI effect. The question  
28 is therefore to know if it is possible to make them fluorescent, without the light emission  
29 being reduced. Indeed, their emission may be quenched due to both the high concentration of  
30 water OH vibrators (Mei et al., 2021) and metal ions in paramagnetic GdCAs (Asberg et al.,  
31 2004) within the nanogels. These nanogels can be made fluorescent by polymer pre-  
32 functionalization. In this work, we have chosen to make these nanogels fluorescent by CS  
33 pre-functionalization. CS backbone was modified at the primary amino group of the  
34 deacetylated CS units (at C-2, Scheme 1) with rhodamine (Rhod) or fluorescein (Fluo)

1 moieties. For that, we have taken advantage of the higher reactivity of the electronic lone pair  
2 of CS primary amino group to graft rhodamine or fluorescein isothiocyanates (RBITC and  
3 FITC respectively) *via* a thiourea linkage. Our objective being to involve those fluorescent CS  
4 in ionic gelation, it is mandatory to control CS degree of substitution (DSCs) after  
5 functionalization. Indeed, sufficient remaining positive charges are necessary on fluorescent  
6 CS backbone to perform subsequent ionic gelation with HA in the presence of an ionogenic  
7 cross linker (Gupta & Jabrail, 2006; Sang et al., 2020). Therefore, CS functionalization with  
8 rhodamine and fluorescein has to be carefully characterized, especially in the absence of an  
9 unambiguous marker of the thiourea bond (Ma et al., 2008). In this context, a series of CS-  
10 fluorophore conjugates (CS-Rhod or CS-Fluo conjugates) were synthesized in which the level  
11 of Rhod or Fluo substitution was systematically varied and quantified by a combination of  
12 fluorescence and DOSY experiments. CS-fluorophores conjugates were then involved in  
13 nanogel synthesis in the presence of GdCAs and after detailed morphological and  
14 toxicological characterizations, the efficacy of the corresponding fluorescent Gd nanogels as  
15 potential magneto-optical nanoprobe was explored.

## 16 1. Materials and Methods

### 17 1.1. Materials

18 Chitosan (CS, from shrimp shells, 51 kDa, viscosity = 33mPa.s in 1% acetic acid, 20°C) was  
19 purchased from Sigma-Aldrich. A deacetylation degree (DD) of 86% was determined by <sup>1</sup>H  
20 NMR spectroscopy according to published procedures. (Hirai et al., 1991; Vårum et al., 1991)  
21 For calculations, CS repetitive unit (rep unit) molecular mass in which CS DD was taken into  
22 account, was considered to be  $M_w$  in average ( $CS_{rep\ unit} = 200\ g.mol^{-1}$ ) (Courant et al., 2012).  
23 Hyaluronic acid sodium salt (HA 1000 kDa extracted from *Streptococcus equi sp*), Rhodamine  
24 B isothiocyanate (RBITC, No. R1755), Fluorescein isothiocyanate (FITC), acetic acid and  
25 sodium acetate were purchased from Sigma-Aldrich. Sodium tripolyphosphate (TPP) was  
26 purchased from Acros Organics. DC1 (35 wt % in D<sub>2</sub>O) and D<sub>2</sub>O were provided from Sigma-  
27 Aldrich and Euriso-top, respectively. HGdDOTA (Gadolinium(III)-1.4.7.10-  
28 Tetraazacyclododecane-1.4.7.10-tetraacetate) was synthesized according a published  
29 procedure (Courant et al., 2012).  
30 Fetal bovine serum (FBS), heat inactivated was purchased from Gibco by Life Technologies  
31 (New Zealand), Roswell Park Memorial Institute (RPMI) 1640 medium and Dulbecco's  
32 Modified Eagle's Medium (DMEM) from Gibco (Invitrogen, Grand Island, N.Y., USA), 3-  
33 (4,5-dimethylthiazol-2-yl)-2,5-diphenyltetrazolium bromide (MTT), *In Vitro* Toxicology

1 Assay Kit Lactic Dehydrogenase based and antibiotics (penicillin, streptomycin and  
2 amphotericin B) were provided by Sigma-Aldrich (St. Louis, MO, USA). Sterile water for  
3 injections (Laboratoire Aguettant, Lyon, France) was systematically used for polymer,  
4 nanoparticle preparations and analyses.

5 All products were used as received, without further purification.

6 Native and functionalized polymers (CS, CS-Rhodamine namely CS-Rhod and CS-  
7 Fluorescein namely CS-Fluo, respectively) were characterized by FTIR (Nicolet IS 5  
8 spectrometer equipped with an ATR ID5 module),  $^1\text{H}$  NMR (Bruker Avance III 500 MHz  
9 NMR spectrometer) at 318 K with  $\text{D}_2\text{O}/\text{DCl}$  (700/1, v/v) as solvent, UV-visible and  
10 fluorescence spectroscopies (Varian Cary 5000 Shimadzu UV-2401PC and Varian Cary  
11 Eclipse, respectively). Centrifugation experiments were performed with an Alegra X-30  
12 centrifuge (Beckman-Coulter).

13 The diffusion coefficients of different materials (CS, RBITC, FITC, CS-Rhod and CS-Fluo)  
14 were determined by DOSY experiments (Diffusion Ordered Spectroscopy) on a Bruker  
15 Avance II 500 MHz NMR spectrometer.

## 16 2.2. Preparation, IR and $^1\text{H}$ NMR characterizations of CS-Rhodamine and CS-Fluorescein 17 polymers

### 18 2.2.1. CS-Rhodamine (CS-Rhod) synthesis

19 CS (200 mg, 1.0 mmol of  $\text{NH}_2$  function) was dissolved under  $\text{N}_2$  atmosphere in 10 mL of an  
20 aqueous solution of acetic acid 1% (v/v). After complete CS dissolution, the pH was adjusted  
21 to 5 by addition of 1M NaOH and 5 mL of MeOH was added and the resulting solution  
22 allowed to stir for 3h (Ma et al., 2008). Then, different stoichiometric ratios of RBITC were  
23 added in anhydrous MeOH to the CS solution (RBITC/ $\text{NH}_2$  CS molar ratio expressed as %  
24 mol  $(\text{NCS}/\text{NH}_2)_{\text{initial}}$  of 2, 5 and 10%, corresponding to 11, 27 and 53 mg of RBITC in 3.5, 8  
25 and 16 mL of anhydrous MeOH respectively). The RBITC solution was added dropwise to  
26 the CS solution and the mixture was stirred under  $\text{N}_2$  atmosphere, in the dark at room  
27 temperature for 36h. At the end of the reaction, CS-Rhod was precipitated by using a NaOH  
28 solution (1M), and the resulting precipitate washed with water for injection. The polymer was  
29 recovered by centrifugation (6500 rpm, 12 min, at room temperature) and the overall  
30 procedure repeated until waste water reached pH 7 and no fluorescence being detected in the  
31 corresponding solution. CS-Rhod was finally obtained after freeze-drying as a pink-mauve  
32 foam (between 120 and  
33 180 mg according to the sample).

1 FT-IR (ATR,  $\text{cm}^{-1}$ ): 3362 ( $\nu_{\text{OH}}$  and  $\nu_{\text{NH}}$ ), 2871 ( $\nu_{\text{CH}}$ ), 1650 (amide I), 1559 (amide II), 1053,  
2 1027 (pyranose ring).

3  $^1\text{H}$  NMR (500 MHz, 318K,  $\text{D}_2\text{O}/\text{DCl}$ : 700  $\mu\text{L}/1\mu\text{L}$ ),  $\delta$  (ppm): 1.30 (t,  $\text{CH}_3$  - Rhod), 2.07 (s,  
4  $\text{CH}_3$  - CS acetyl units), 2.99 (s, 1H, CS), 3.37 (s,  $\text{CH}_2$  - Rhod), 3.5-4.2 (m, 5H, CS), 4.71 (s,  
5 1H, CS), 6.9-7.9 (aromatic H - Rhod).

### 6 2.2.2. CS-Fluorescein (*CS-Fluo*) synthesis

7 CS-Fluorescein (CS-Fluo) was synthesized according to the same procedure, *i.e.* from a CS  
8 solution (mixture of acetic acid and anhydrous MeOH) and FITC solution (in anhydrous  
9 MeOH). The same FITC/ $\text{NH}_2$  CS molar ratios were prepared namely 2, 5 and 10% (expressed  
10 as % mol ( $\text{NCS}/\text{NH}_2$ )<sub>initial</sub>) corresponding to 8, 20 and 40 mg of FITC in 3, 7.5 and 15 mL of  
11 anhydrous MeOH respectively.

12 After precipitation (with 1 M NaOH) and washing with water for injection until pH 7, CS-  
13 Fluo was finally obtained after freeze-drying as an orange foam (between 130 and 180 mg  
14 according to the sample).

15 FT-IR (ATR,  $\text{cm}^{-1}$ ): 3288 ( $\nu_{\text{OH}}$  and  $\nu_{\text{NH}}$ ), 2874 ( $\nu_{\text{CH}}$ ), 1634 (amide I), 1573 (amide II), 1063,  
16 1028 (pyranose ring).

17  $^1\text{H}$  NMR (500 MHz, 318K,  $\text{D}_2\text{O}/\text{DCl}$ : 700  $\mu\text{L}/1\mu\text{L}$ ),  $\delta$  (ppm): 2.07 (s,  $\text{CH}_3$  - CS acetyl units),  
18 3.02 (s, 1H, CS), 3.5-4.2 (m, 5H, CS), 4.73 (s, 1H, CS), 6.5-8.0 (aromatic H - Fluo).

### 19 2.3. Determination of CS degree of substitution ( $DS_{\text{CS}}$ ) by a combination of fluorescence 20 and DOSY experiments

21 In order to determine the degree of substitution of chitosan in CS-Rhod ( $DS_{\text{CS}}^{\text{Rhod}}$ ) or CS-Fluo  
22 ( $DS_{\text{CS}}^{\text{Fluo}}$ ) samples, it was mandatory to distinguish between the grafted amount of fluorophore  
23 (RBITC<sub>G</sub> namely Rhod<sub>G</sub> or FITC<sub>G</sub> namely Fluo<sub>G</sub>) and the ungrafted one (Rhod<sub>UG</sub> or Fluo<sub>UG</sub>).  
24 For that, a combination of fluorescence spectroscopy and DOSY experiments was applied.

25 *Fluorescence spectroscopy*: The total amount of fluorophore (Rhod<sub>T</sub> or Fluo<sub>T</sub>) which  
26 corresponded to the sum of the grafted fluorophore amount (Rhod<sub>G</sub> or Fluo<sub>G</sub>) and the  
27 ungrafted one (Rhod<sub>UG</sub> or Fluo<sub>UG</sub>), was determined by fluorescence spectroscopy after sample  
28 purification. For this purpose, we measured the emission intensities at 576 nm (rhodamine) or  
29 511 nm (fluorescein) of 0.25-0.45 mg  $\text{mL}^{-1}$  solutions of CS-Rhod (or CS-Fluo), dissolved in  
30 an aqueous solution of acetic acid 1% (v/v) and diluted 100 times with acetate buffer (pH 4.7)  
31 (Varian Cary Eclipse spectrometer, with  $\lambda_{\text{exc}}$  = 550 and 450 nm for rhodamine and fluorescein

1 emission measurements respectively, and  $\Delta\lambda_{exc} = \Delta\lambda_{em} = 5$  nm). The ratio of the total amount  
 2 of fluorophore to chitosan (fluorophore<sub>T</sub>/ CS) was calculated as the percent molar  
 3 concentration of fluorophore to CS molar concentration according to Eq. 1.

$$4 \quad \% \left( \frac{\text{fluorophore}_T}{CS} \right)_{mol} = \frac{I_{\text{fluorophore}}/k_{\text{fluorophore}}}{m_{CS\text{-fluorophore}}/(M_{CS_{rep\ unit}} \times V)} \times 100 \quad Eq. 1$$

5 with  $I_{\text{fluorophore}}$  being the emission intensity measured at 576 and 511 nm for CS-Rhod and CS-  
 6 Fluo respectively,  $k_{\text{fluorophore}}$  being equal to the ratio between the emission intensity (at 576 or  
 7 511 nm) and the fluorophore concentration.  $k_{\text{fluorophore}}$  was determined for rhodamine and  
 8 fluoresceine by calibration with standard solutions of each fluorophore. Serial dilutions in  
 9 acetate buffer (pH 4.7) of a stock methanolic solution of each fluorophore (150 mg mL<sup>-1</sup>)  
 10 were prepared to reach fluorophore concentrations ranging from 0.003 to 0.1 mg mL<sup>-1</sup>. The  
 11 corresponding proportionality coefficient determined were  $k_{\text{Rhod}, 576 \text{ nm}} = 1.75 \times 10^9$  mol<sup>-1</sup>L  
 12 and  $k_{\text{Fluo}, 511 \text{ nm}} = 4.58 \times 10^8$  mol<sup>-1</sup>L.

13 *DOSY Experiments:* Due to the large difference between rhodamine (or fluorescein) and CS-  
 14 Rhod (or CS-Fluo) molecular weights, it was expected to discriminate between ungrafted and  
 15 grafted fluorophore, using their respective diffusion coefficients. For that, preliminary DOSY  
 16 experiments were performed to determine CS, rhodamine (Rhod) and fluorescein (Fluo)  
 17 diffusion coefficients ( $D_{CS}$ ,  $D_{\text{Rhod}}$  and  $D_{\text{Fluo}}$  respectively). Bipolar gradient pulses with two  
 18 spoil gradients were used to measure these coefficients (BPP-LED pulse sequence). The value  
 19 of the gradient pulse length  $\tau$  was 4 ms for CS and 2ms for Rhod and Fluo, while the value of  
 20 the diffusion time  $\Delta$  was set to 500 ms for CS and 250 ms for Rhod and Fluo. The pulse  
 21 gradients were incremented in 16 steps from 2% to 95% of the maximum gradient strength  
 22 (53.5 G/cm) in a linear ramp and the temperature was set at 30°C. CS, Rhod and Fluo  
 23 diffusion curves were then extracted from DOSY spectra of CS (for the peak at  
 24  $\delta = 2.1$  ppm), Rhod (for the peak at  $\delta = 1.2$  ppm) and Fluo (for the peak at  $\delta = 6.8$  ppm). In  
 25 each case, the mono-exponential diffusion curves were fitted with Eq. 2 (Johnson, 1999;  
 26 Augé, Amblard-Blondel & Delsuc, 1999) to obtain  $D_{CS}$  value of  $5 \times 10^{-12}$  m<sup>2</sup>s<sup>-1</sup>, and  $D_{\text{Rhod}}$  and  
 27  $D_{\text{Fluo}}$  values of  $2 \times 10^{-10}$  m<sup>2</sup>s<sup>-1</sup> and  $4 \times 10^{-10}$  m<sup>2</sup>s<sup>-1</sup> respectively (Figure S4).

$$28 \quad I = I_0 \exp[-\gamma^2 g^2 D \delta^2 (\Delta - (\delta/3) - (\tau/2))] \quad Eq. 2$$

29 Then, similar DOSY experiments were performed with CS-Rhod and CS-Fluo. The diffusion  
 30 curves were extracted from CS-Rhod and CS-Fluo DOSY spectra, for the more intense peak  
 31 of Rhod and Fluo, at 1.3 and 6.8 ppm respectively. The diffusion curves that showed a

1 monoexponential evolution were fitted according to Eq. 2. The diffusion curves that exhibited  
 2 a biexponential evolution were fitted according to Eq. 3, (Johnson, 1999; Augé, Amblard-  
 3 Blondel & Delsuc, 1999)

$$4 \quad I = I_G \exp[-\gamma^2 g^2 D_G \mathcal{F}(\Delta - (\delta/3) - (\tau/2))] + I_{UG} \exp[-\gamma^2 g^2 D_{UG} \mathcal{F}(\Delta - (\delta/3) - (\tau/2))] \quad \text{Eq. 3}$$

5 where  $I_G$  and  $I_{UG}$  were the intensities at 0% gradient, for grafted and ungrafted fluorophore  
 6 (Rhod or Fluo) respectively,  $\gamma$  the gyromagnetic ratio,  $g$  the gradient strength,  $D_G$  and  $D_{UG}$  the  
 7 diffusion coefficients of grafted and ungrafted fluorophores respectively,  $\delta$  the gradient pulse  
 8 length,  $\Delta$  the diffusion time and  $\tau$  the interpulse spacing in the BPP-LED pulse sequence.

9 During the fitting,  $D_G$  and  $D_{UG}$  were then fixed to values measured independently on chitosan  
 10 and rhodamine or fluorescein, respectively:  $D_{CS} = 5 \times 10^{-12} \text{ m}^2\text{s}^{-1}$ ,  $D_{Rhod} = 2 \times 10^{-10} \text{ m}^2\text{s}^{-1}$  and  
 11  $D_{Fluo} = 4 \times 10^{-10} \text{ m}^2\text{s}^{-1}$ .

12  $I_G$  and  $I_{UG}$  values extracted from the fitting, allowed to calculate the percentage of grafted  
 13 fluorophore over the total amount of fluorophore (fluorophore<sub>G</sub>/fluorophore<sub>T</sub>) (Eq. 4):

$$14 \quad \% \frac{\text{Fluorophore}_G}{\text{Fluorophore}_T} = \frac{I_G}{I_G + I_{UG}} \times 100 \quad \text{Eq. 4}$$

15 The percentage of fluorophore grafted to CS chains ( $DS_{CS}$ ) was then calculated (Eq. 5) from  
 16 emission measurements and DOSY experiments (from Eqs. 1 and 4):

$$17 \quad DS_{CS} = \% \left( \frac{\text{fluorophore}_G}{CS} \right) = \frac{I_{\text{fluorophore}}/k_{\text{fluorophore}}}{m_{CS-\text{fluorophore}}/(M_{CS_{rep\ unit}} \times V)} \times \frac{I_G}{I_G + I_{UG}} \times 100 \quad \text{Eq. 5}$$

18 where  $I_G$  and  $I_{UG}$  stand for the intensities extracted from the DOSY experiments, for grafted  
 19 and ungrafted fluorophores (rhodamine or fluorescein) respectively.

## 20 *2.4. Preparation and characterization of CS–Rhod and CS–Fluo nanoparticles by ionic* 21 *gelation (CS–Rhod-TPP/HA and CS–Fluo-TPP/HA nanogels)*

### 22 *2.4.1. CS–Rhod-TPP/HA and CS–Fluo-TPP/HA nanogel syntheses*

23 Solutions of fluorescent CS were prepared by dissolution of CS-Rhod ( $DS_{CS}^{Rhod} = 0.85\%$ ) or  
 24 CS-Fluo ( $DS_{CS}^{Fluo} = 0.86\%$ ) powders in citric acid (10% wt/v) solutions (2.5 mg mL<sup>-1</sup>).

25 CS-fluorophore-TPP/HA nanogels (CS–Rhod-TPP/HA and CS–Fluo-TPP/HA NGs) were  
 26 obtained by an ionotropic gelation process. For this purpose, the polyanionic aqueous phase  
 27 (4.5 mL) containing both HA (0.8 mg mL<sup>-1</sup>) and TPP (1.2 mg mL<sup>-1</sup>) was added dropwise to  
 28 the CS-fluorophore solution (9 mL) under sonication (750W, amplitude 32%). At the end of  
 29 the addition, magnetic stirring was maintained for 10 min. Purification and pH correction of  
 30 the nanosuspensions was then carried out by dialysis against water for injection (3 × 12h)

1 using a membrane of 25 kDa cut-off (Spectrum Lab) to reach physiological pH. Gadolinium-  
2 loaded nanogels (GdDOTA $\subset$ CS-Rhod-TPP/HA and GdDOTA $\subset$ CS-Fluo-TPP/HA NGs) were  
3 prepared in the same way, by incorporating HGdDOTA (17 mg) as the MRI contrast agent in  
4 the anionic phase.

#### 5 2.4.2. CS–Rhod and CS–Fluo nanogels characterization by Dynamic Light Scattering

6 The nanogels averaged hydrodynamic diameters (Z-ave) were determined by Dynamic Light  
7 Scattering (DLS) with a Zetasizer Nano ZS (Malvern Zetasizer Nano-ZS, Malvern  
8 Instruments, Worcestershire, UK). Each sample was analyzed in triplicate at 20 °C at a  
9 scattering angle of 173°, after a 1/20 dilution in water. Water was used as a reference  
10 dispersing medium.

11  $\zeta$ -(zeta) potential data were collected through Electrophoretic Light Scattering (ELS) at 20°C,  
12 150 V, in triplicate for each sample, after a 1/20 dilution in water. The instrument was  
13 calibrated with a Malvern – 68 mV standard before each analysis cycle.

#### 14 2.4.3. In vitro cytotoxicity of CS-Rhod and CS-Fluo nanogels

15 RAW 267.4 and A20 cell lines were purchased from American Type Culture Collection  
16 (ATCC catalog no., TIB-7 and TIB-208, respectively). RAW 267.4 cells (adherent cells) were  
17 cultured in Dulbecco Modified Eagle Medium (DMEM) pH 7.4 with 4 mM L-glutamine  
18 adjusted to contain 4.5 g L<sup>-1</sup> glucose and, 1.5 g L<sup>-1</sup> sodium bicarbonate. The growth medium  
19 was supplemented with 10% fetal bovine serum, 1% antibiotics (penicillin, streptomycin,  
20 amphotericin). The A20 cell line (murine B lymphocytes, from reticulum cell sarcoma in  
21 suspension) were cultured in RPMI 1640 medium pH 7.4 with 2 mM L-glutamine, 1.5 g L<sup>-1</sup>  
22 Na<sub>2</sub>CO<sub>3</sub>, 4.5 g L<sup>-1</sup> glucose, 1 mM sodium pyruvate, 10 mM HEPES and supplemented with  
23 10% fetal bovine serum and 1% antibiotics (penicillin, streptomycin, and amphotericin). All  
24 cell types were maintained at 37°C in a humidified atmosphere (95%) with 5% CO<sub>2</sub>.  
25 The concentration of CS-Rhod-TPP/HA and CS-Fluo-TPP/HA stock nanosuspensions was  
26 1.17 mg mL<sup>-1</sup> and the Gd concentration of GdDOTA $\subset$ CS-Rhod-TPP/HA and GdDOTA $\subset$ CS-  
27 Fluo-TPP/HA stock nanosuspensions was 0.144 mM and 0.144 mM respectively. Dilutions  
28 were then made in the culture medium for each cell line tested. In parallel, the cells seeded in  
29 24-well plates at a density of 10<sup>5</sup> cells mL<sup>-1</sup> for RAW 264.7 and 2×10<sup>5</sup> cells mL<sup>-1</sup> for A20 cell  
30 lines, were incubated for 6 and 24 hours at different concentrations of CS-Rhod-TPP/HA, CS-  
31 Fluo-TPP/HA nanogels (*i.e.* 5, 15, 30, 60 and 120  $\mu$ g mL<sup>-1</sup>) or GdDOTA $\subset$  CS-Rhod-TPP/HA  
32 and GdDOTA $\subset$ CS-Fluo-TPP/HA nanogels (*i.e.* 0.5, 1, 2.5, 5 and 10  $\mu$ M of Gd).

1 Cell viability was measured by the MTT, 3-(4,5-dimethylthazol-2-yl)-2,5-diphenyl  
2 tetrazolium bromide), assay. After the exposure time, the culture medium was removed and in  
3 each well were added 500  $\mu\text{L}$  MTT ( $1 \text{ mg mL}^{-1}$ ) for 2 hours. After that, the MTT solution was  
4 removed and the formazan crystals were solubilized in 100% isopropanol. The optical density  
5 was measured at 595 nm using Flex Station 3 Multi-Mode Microplate Reader. The cell  
6 viability was expressed in percentage considering 100% viability for control cells.

7 The LDH release was measured in the culture media of treated cells using the *In Vitro*  
8 Toxicology Assay Kit (Sigma-Aldrich, USA) and compared to the LDH release level of  
9 control (untreated cells). After each exposure interval, a volume of 50  $\mu\text{L}$  medium was taken  
10 from each sample and placed on a 96-well microtiter plate and then 100  $\mu\text{L}$  of assay mixture  
11 were added. After 20-30 min at room temperature, the reaction was stopped by adding 1/10  
12 volume of HCl 1 M and the enzymatic activity was determined spectrophotometrically using  
13 the Flex Station 3 Multi-Mode Microplate Reader. The absorbance was read at 450 nm and  
14 the results were expressed relative to control.

#### 15 2.4.4. Fluorescent nanogels characterization by Atomic Force Microscopy (AFM) and 16 confocal microscopy

17 To obtain information about the different NP sizes and their fluorescent properties, correlative  
18 experiments were performed using an Atomic Force Microscope (AFM) coupled to a confocal  
19 microscope. Each sample was analyzed in triplicate at 20 °C after a 1/20 dilution in water. To  
20 be observed, the NPs were deposited on a glass slide and after one hour, the samples were  
21 rinsed with deionized water. All the experiments were performed in water to avoid nanogel  
22 drying (and thus possible changes in their structures / morphologies).

23 First a confocal image was acquired using a Axio Observer 7 LSM 800 Airyscan microscope  
24 (ZEISS, Germany). For the excitation wavelength, lasers at 561 and 488 nm were used for the  
25 CS-Rhod-TPP/HA and CS-Fluo-TPP/HA nanogels, respectively. A 100 $\times$  objective was used  
26 and 512 pixels  $\times$  512 pixels image were acquired. Then in a second time, areas with  
27 fluorescent NPs were chosen and scanned with a Resolve AFM (BrukerNano, USA). Peak  
28 Force Tapping Quantitative Nano-Mechanicals (PFT-QNM) mode was used to perform AFM  
29 imaging of the different samples in liquid conditions. Nitride coated silicon cantilevers (SNL,  
30 Bruker probes, USA) with a resonance frequency of 65 kHz, a nominal spring constant of  
31 0.35 N/m and a tip radius of 6 nm were used for this work and were calibrated for each  
32 experiment. Images were acquired with a scan rate of  $\sim 1.0 - 1.5$  Hz, with a force kept as low  
33 as possible (typically 0.5 nN or lower). Imaging gains were automatically optimized by the

1 software. The different AFM images were analyzed and processed with the Nanoscope  
2 Analysis 2.0 software (BrukerNano, USA). At least, 5 different areas for each sample were  
3 analyzed by AFM to determine averaged NP diameters.

#### 4 *2. 5. Determination of the gadolinium concentration in nanogels by ICP-OES*

5 Gadolinium nanoparticle loading was determined on purified and concentrated  
6 nanosuspensions by Inductively Coupled Plasma - Optical Emission Spectroscopy (ICP-  
7 OES). The non-encapsulated complexes were separated from the NGs by high speed  
8 centrifugation for 1 h 15 min at 4°C and 23 200 g (Beckman Avanti™ J-E Centrifuge,  
9 France). The NP pellet was then incubated overnight in a 1:3 (v/v) mixture of HCl (37%) and  
10 HNO<sub>3</sub> (69%) in order to release Gd from the polymer matrix and the complexes. After the NG  
11 destruction, volumetric dilutions were carried out to achieve an appropriate Gd concentration  
12 within the detection range of the method. Similar procedure was implemented to determine  
13 Gd content in supernatants. Samples were analyzed using ICAP 6000 series ICP-OES  
14 spectrometer. Counts of Gd were correlated to a Gd calibration curve generated by mixing  
15 Gd(NO<sub>3</sub>)<sub>3</sub> standard with unloaded NGs incubated under the same acidic conditions.

#### 16 *2.6. Evaluation of fluorophore concentration in nanogels by fluorescence spectroscopy.*

17 Rhodamine or fluorescein concentrations were determined by fluorescence (Varian Cary  
18 Eclipse spectrometer) on dialysed nanogels, after high speed centrifugation (23 200 g, 1 h 15,  
19 4°C) both in NP pellets and in supernatants, using the same methodology as the one used for  
20 the determination of fluorophore concentrations on CS-Rhod and CS-Fluo polymers.

#### 21 *2.7. Relaxivity measurements*

22 *NMRD profiles.* <sup>1</sup>H NMRD profiles were measured on a Stellar Spinmaster FFC fast field  
23 cycling NMR relaxometer (Stellar, Mede, Pavia, Italy) over a range of magnetic fields  
24 extending from 0.24 mT to 0.7 T and corresponding to <sup>1</sup>H Larmor frequencies from 0.01 to 30  
25 MHz using 0.6 mL samples in 10 mm o.d. tubes. The temperature was kept constant at 37°C.  
26 An additional relaxation rate at 60 MHz was obtained with a Bruker Minispec mq60  
27 spectrometer (Bruker, Karlsruhe, Germany). The diamagnetic contribution of unloaded  
28 particles was measured and subtracted from the observed relaxation rates of the Gd-loaded  
29 nanoparticles.

30 *MR Imaging.* MR imaging of NP suspensions were performed using a 3.0 T MRI device  
31 (Skyra, Siemens Healthcare, Erlangen, Germany) with a 15 channel transmit/receive knee  
32 coil. *T*<sub>1</sub>-weighted images were obtained with an 3D fast spin-echo *T*<sub>1</sub> sequence (TR = 700 ms,  
33 TE = 12 ms, FOV = 201×201 mm, matrix= 256×256, voxel size = 0.78×0.78×2mm). *T*<sub>2</sub>-

1 weighted images were obtained with an 3D fast spin-echo  $T_2$  sequence (TR = 1000 ms, TE =  
2 103 ms, FOV =  $199 \times 199$  mm, matrix =  $384 \times 384$ , voxel size =  $0.52 \times 0.52 \times 0.55$ mm). The  
3 gadolinium concentrations were tested in the 25–200  $\mu$ M range.

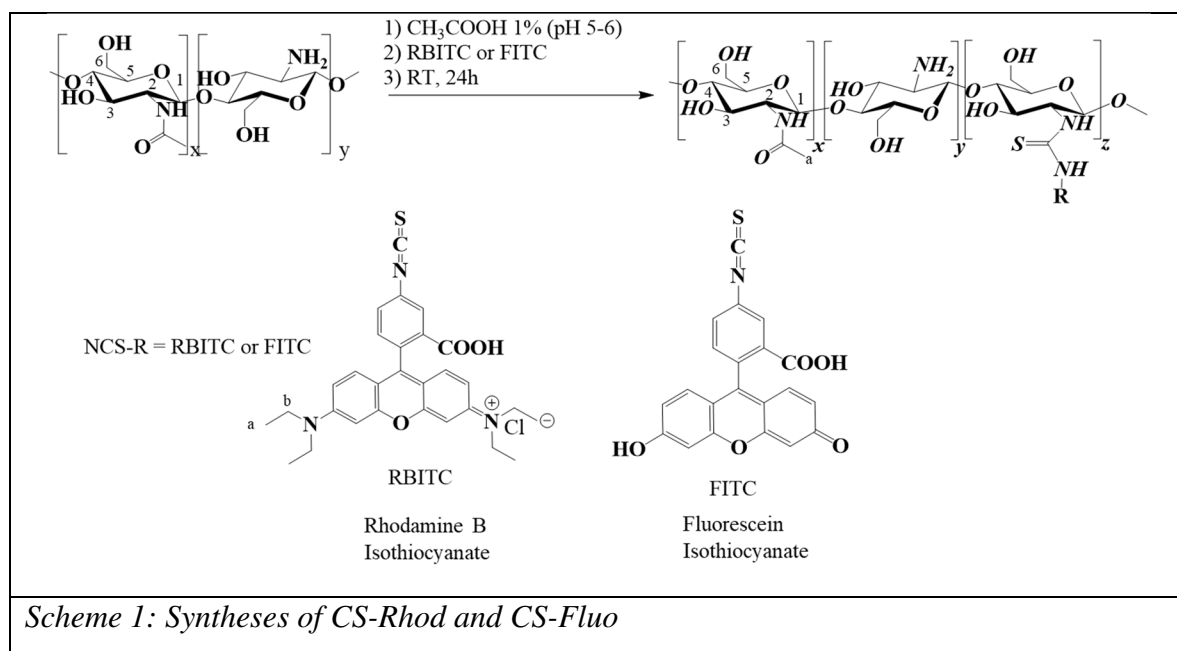
4

5

6

## 1 Results and Discussion

### 2 1.2. Preparation and characterization of CS grafted with Rhodamine B Isothiocyanate 3 (CS-Rhod) and Fluorescein Isothiocyanate (CS-Fluo)



4 The functionalization of chitosan (CS) by conventional fluorophores, namely RBITC and  
5 FITC that emitted in red and green regions respectively, was performed by a direct coupling  
6 between the fluorophore isothiocyanate group and the amino function of the CS glucosamine  
7 residue. (Ma et al., 2018) To optimize the labelling procedure, several initial molar ratios  
8 (NCS/ $\text{NH}_2$ ), chosen between 2 and 10% for each fluorophore, were used in order to provide  
9 sufficient grafting yields while avoiding optical signal saturation. After workup and freeze-  
10 drying, fluorescent CS samples were characterized by UV-visible and emission  
11 spectroscopies, FT-IR and  $^1\text{H}$  NMR at 318 K ( $\text{D}_2\text{O}/\text{DCl}$  as solvent). The absorption and  
12 fluorescence maxima in water medium of CS-Rhod were located at 550 nm and 576 nm,  
13 respectively, and the ones of CS-Fluo were located at 450 nm and 511 nm, respectively  
14 (Figure 1). They were similar to those of the free dyes (Leng et al., 2017; Xia et al., 2016).  
15 FT-IR spectra of CS-Rhod and CS-Fluo samples (Figure S1) showed the disappearance of the  
16 FT-IR band at  $2030\text{-}2150\text{ cm}^{-1}$  attributed to the isothiocyanate group (Sinagaglia et al., 2012).  
17 These data suggested the involvement of the thiourea moiety in the conjugation of both  
18 fluorophores with CS.

19

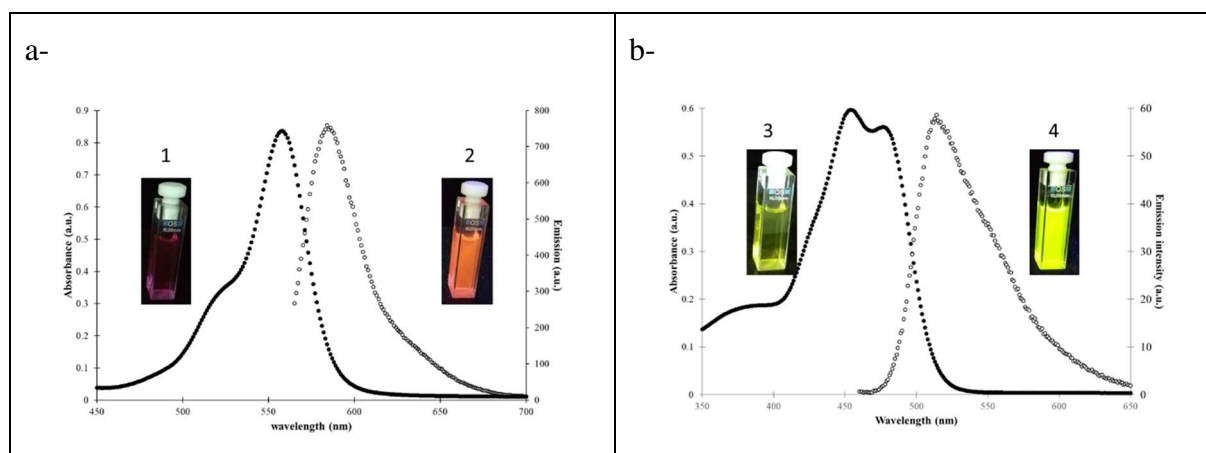


Figure 1: Absorbance (●) and emission (○) spectra of in acetate buffer (pH 4.7), (a) CS-Rhod; (b) CS-Fluo, % mol  $(\text{NCS}/\text{NH}_2)_{\text{initial}} = 10\%$ . Optical images of CS-Rhod and CS-Fluo under natural light (pictures 1 and 3, respectively) and under UV light (365 nm, pictures 2 and 4, respectively).

1 Similarly,  $^1\text{H}$  NMR spectra of CS-Rhod and CS-Fluo (Figure S2), in addition to chemical  
 2 shifts corresponding to CS backbone or acetyl protons ( $\text{H}_2$  of pyranose ring at  
 3  $\delta = 3.0$  ppm,  $\text{H}_3$  to  $\text{H}_6$  of pyranose ring at  $\delta = 3.5\text{-}4.2$  ppm, anomeric  $\text{H}_1$  at  $\delta = 4.7$  ppm and  
 4 acetyl protons at  $\delta = 2.1$  ppm), confirmed the presence of rhodamine moiety in CS-Rhod  
 5 samples (Figure S2a -  $\text{H}_a$  at  $\delta = 1.3$  ppm,  $\text{H}_b$  at  $\delta = 3.4$  ppm, and  $\text{H}_{ar}$  at  $\delta = 6.9\text{-}7.9$  ppm) as  
 6 well as fluorescein moiety in CS-Fluo samples (Figure S2b -  $\text{H}_{ar}$  at  $\delta = 6.5\text{-}8.0$  ppm).  
 7 In the absence of a spectroscopic marker specific to the thiourea linkage, the evaluation of CS  
 8 degree of substitution ( $\text{DS}_{\text{CS}}$ ) post-grafting, cannot be given by the sole  $^1\text{H}$  NMR spectra  
 9 analyses since they only help to determine the total amount of fluorophore associated to CS.  
 10 Indeed, in CS-Rhod samples this amount ( $\text{Rhod}_T$ ) could be determined by the ratio between  
 11 the integration of  $\text{H}_a$  rhodamine  $^1\text{H}$  signal (divided by 12) and chitosan signals ( $\text{H}_2$  CS  $^1\text{H}$   
 12 signal which was set to 1). Similar analysis could be performed for CS-Fluo, the total amount  
 13 of fluorescein associated to CS ( $\text{Fluo}_T$ ) being obtained *via* the ratio between the integration of  
 14 fluorescein aromatic  $^1\text{H}$  (divided by 9) and chitosan signals ( $\text{H}_2$  CS  $^1\text{H}$  signal always set to 1).  
 15 Unfortunately for the lowest initial  $(\text{NCS}/\text{NH}_2)$  molar ratio (2%), the  $^1\text{H}$  signals associated to  
 16 each fluorophore were too weak to be integrated with accuracy. To circumvent this drawback,  
 17 the total amount of each optical probe was determined by fluorescence and this, for each  
 18  $(\text{NCS}/\text{NH}_2)$  initial ratio (*Eq. 1* Experimental Section). The results obtained from fluorescence  
 19 spectroscopy showed that after workup, the total amount of rhodamine ( $\text{Rhod}_T$ ) associated to  
 20 CS were 0.18, 0.44 and 1.03% for  $(\text{NCS}/\text{NH}_2)$  initial ratios of 2, 5 and 10%, respectively  
 21 (Table S3), the total amount of fluorescein ( $\text{Fluo}_T$ ) associated to CS being 0.22, 0.54 and  
 22 1.02% for the same  $(\text{NCS}/\text{NH}_2)$  initial ratios, respectively. These data indicated then that only

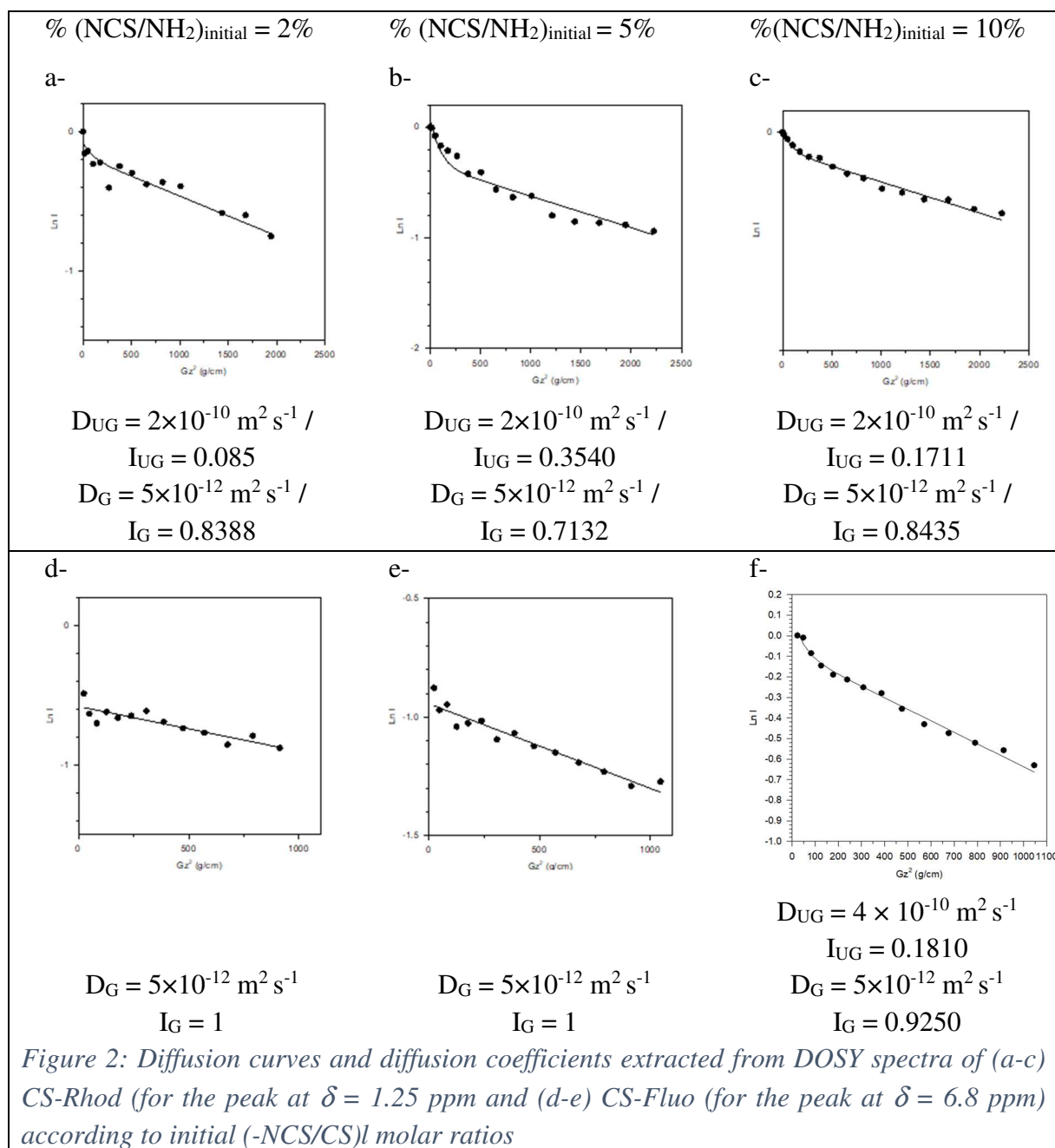
1 10% of the probe (Rhod or Fluo) initially introduced remained associated to CS after reaction,  
2 which highlighted the efficiency of purification step.

3 In order to properly evaluate the amount of grafted fluorophore (Rhod<sub>G</sub> or Fluo<sub>G</sub>), CS-Rhod  
4 and CS-Fluo samples were subjected to DOSY experiments (Belabassi et al., 2017).

5 In the case of CS-Rhod polymers, these curves extracted from CS-Rhod DOSY spectra were  
6 clearly non-linear (Figures 2 a-c). Their biexponential shape highlighted in these samples the  
7 presence of two contributions, one coming from the ungrafted rhodamine (Rhod<sub>UG</sub>) which  
8 diffused faster than the second one coming from grafted rhodamine to CS chains (Rhod<sub>G</sub>).

9 Due to first the large difference between rhodamine and CS molecular weights and second  
10 taking into account the weak percentages determined by fluorescence of fluorophores  
11 associated to the polymer chains (*vide supra*), one can assume that fluorophore grafting  
12 should not restrict CS chain mobility and consequently, CS-Rhod molecular weight must be  
13 close to the one of CS. Therefore, a bi-exponential fitting of these curves was performed  
14 (Eq.3), for which two diffusion coefficients of  $2 \times 10^{-10} \text{ m}^2 \text{ s}^{-1}$  (for Rhod<sub>UG</sub>, Figure S4) and  
15  $5 \times 10^{-12} \text{ m}^2 \text{ s}^{-1}$  (for CS, Figure S4 and then CS-Rhod) were used.

16



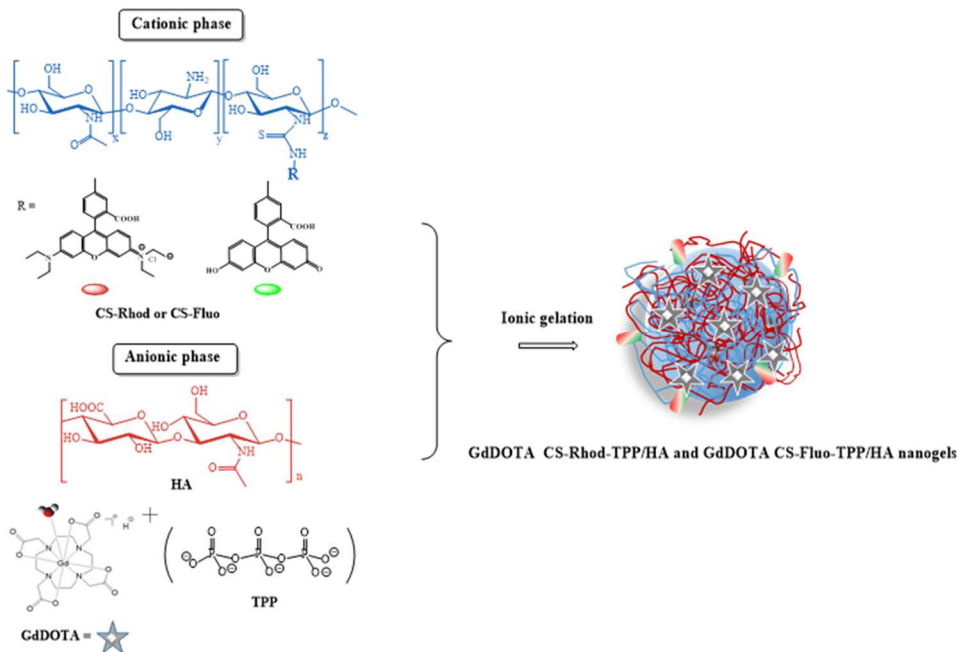
2 In the case of CS-Fluo polymers, the diffusion curves extracted from DOSY spectra were  
3 linear for the two first ratios (2 and 5%) and clearly non-linear for the last one (10%) (Figures  
4 2 d-f). For the two first cases, a mono-exponential fitting was considered (Eq.2) which led to a  
5 diffusion coefficient close to the one measured on chitosan alone, meaning that 100 % of the  
6 fluorophore present was grafted to chitosan. For the third one, a bi-exponential fitting was  
7 performed for which two diffusion coefficients of  $4 \times 10^{-10} \text{ m}^2 \text{ s}^{-1}$  (for Flu<sub>UG</sub>, Figure S4) and  
8  $5 \times 10^{-12} \text{ m}^2 \text{ s}^{-1}$  (for CS, Figure S4 and then CS-Fluo) were fixed. Thus, the curves fitting  
9 allowed to extract the percentage of grafted fluorophore over their total amount  
10 (Rhod<sub>G</sub>/Rhod<sub>T</sub> and Flu<sub>G</sub>/Flu<sub>T</sub>, Eq. 4).

1 According to the initial molar ratio, Rhod<sub>G</sub>/Rhod<sub>T</sub> ratios were estimated between 67 and 91 %  
 2 while Fluor<sub>G</sub> / Fluor<sub>T</sub> ratios were estimated between 84 and 100 % (Table S3). These results  
 3 indicated that almost all the fluorophores present in fluorescent CS samples were grafted.  
 4 Final DS<sub>CS</sub>, as far as they are concerned, were comprised between 0.16 and 0.86 % (Table S3)  
 5 whatever the fluorophore. This indicated that at least 1% of amino functions were  
 6 functionalized with Rhod or Fluo, and that sufficient protonable amino functions remained  
 7 available to be involved in the preparation of nanoparticles by ionic gelation.

8

9 *1.3. CS-Rhod-TPP/HA and CS-Fluo-TPP/HA nanogel syntheses and characterizations*

10 CS-Rhod with a DS<sub>CS</sub> of 0.85% and CS-Fluo with a DS<sub>CS</sub> of 0.86% were then evaluated for  
 11 their ability to produce fluorescent CS-Rhod-TPP/HA and CS-Fluo-TPP/HA nanogels able to  
 12 encapsulate gadolinium chelate. For that, CS-Rhod and CS-Fluo polymers in association with  
 13 sodium hyaluronate (HA) in the presence of tripolyphosphate (TPP) were used to produce  
 14 under mild conditions and without the use of solvents except water, nanoparticles by ionic  
 15 gelation (Scheme 2). These conditions allowed the development of multivalent electrostatic  
 16 interactions between the polycationic phase constituted of CS derivatives and the polyanionic  
 17 chains of HA (ionic complexation between these polymers), these polymeric chains being  
 18 interconnected by the low-molecular weight cross-linker, TPP. (Berger et al., 2004). With  
 19 each polymer tested, stable and homogeneous nanosuspensions were obtained.



*Scheme 2: CS-Rhod-TPP/HA and CS-Fluo-TPP/HA nanogel syntheses*

1 Gadolinium-loaded nanoparticles were prepared in the same way by incorporating  
 2 HGdDOTA as the MRI contrast agent in the preparation. This macrocyclic gadolinium  
 3 chelate, characterized by a high thermodynamic and kinetic stability, is the active substance of  
 4 DOTAREM®. It is recognized as low-risk towards nephrogenic systemic fibrosis (NSF) in  
 5 renal impaired patients (Khawaja et al., 2015) and its macrocyclic structure helps to prevent  
 6 gadolinium leakage and subsequent deposition in brain (Gianolio et al., 2017). The resulting  
 7 GdDOTA<sub>c</sub>CS-Rhod-TPP/HA or GdDOTA<sub>c</sub>CS-Fluo-TPP/HA nanoparticles (Table 1) had  
 8 similar morphological characteristics as the non-fluorescent ones (Table S5).

9 *Table 1: Intensity weighted (Z-average) diameters, polydispersity indexes (PdI), zeta potential*  
 10 *( $\zeta$ ) and Gd(III) loadings of CS-Rhod-TPP/HA and CS-Fluo-TPP/HA nanogels*

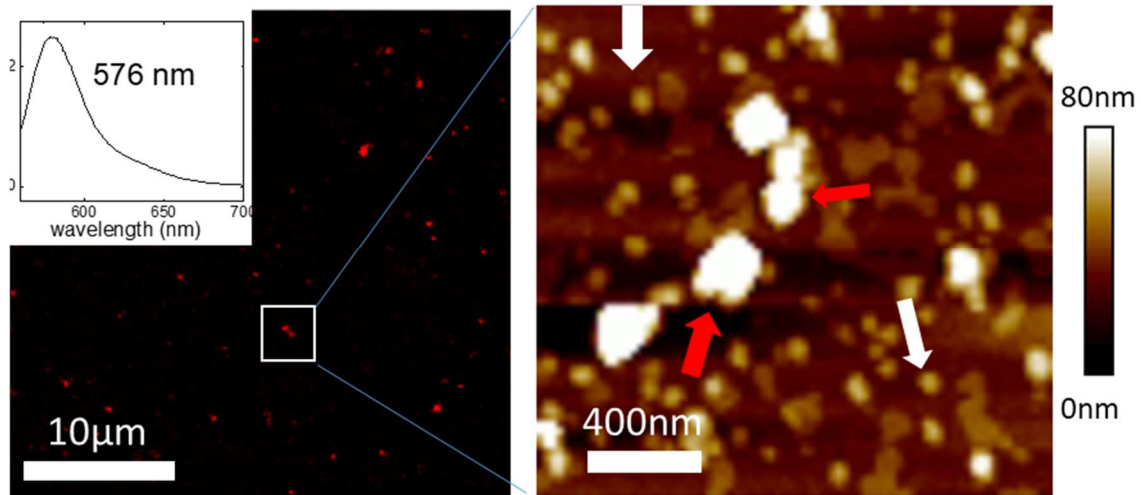
Polymer	Before dialysis			After dialysis				
	Z-ave $\pm$ sd (nm)	PdI $\pm$ sd	$\zeta$ $\pm$ sd (mV)	Z-ave $\pm$ sd (nm)	PdI $\pm$ sd	$\zeta$ $\pm$ sd (mV)	$d_{AFM}$ $\pm$ sd(nm)	[Gd] <sub>NP</sub> (mM)
CS- Rhod	241 $\pm$ 11	0.16 $\pm$ 0.02	49 $\pm$ 1	321 $\pm$ 20	0.22 $\pm$ 0.01	38 $\pm$ 2	65 $\pm$ 13	97
CS-Fluo	195 $\pm$ 10	0.17 $\pm$ 0.01	48 $\pm$ 1	221 $\pm$ 14	0.24 $\pm$ 0.01	35 $\pm$ 1	57 $\pm$ 10	111
CS	219 $\pm$ 10	0.20 $\pm$ 0.01	43 $\pm$ 4	226 $\pm$ 10	0.19 $\pm$ 0.01	35 $\pm$ 1	62 $\pm$ 12	96

11  
 12 ICP-OES analyses of GdDOTA<sub>c</sub>CS-Rhod-TPP/HA or GdDOTA<sub>c</sub>CS-Fluo-TPP/HA  
 13 nanoparticles indicated that their gadolinium loading, around 100 mM, was similar to those of  
 14 GdDOTA<sub>c</sub>CS-TPP/HA controls (Table 1).

15 To characterize the morphology and the optical properties of the fluorescent nanohydrogels,  
 16 confocal images coupled to AFM measurements in liquid were used (Figure 3), thanks to a  
 17 correlative setup. Compared to other types of microscopies, AFM allows to have a high  
 18 resolution while keeping the proper physiological environment and then minimal physical  
 19 perturbations to these fragile samples (which can burn under electronic irradiation for  
 20 instance). From a methodological point of view, it was possible to check first the fluorescent  
 21 properties of the NGs through confocal microscopy and then to focus on a proper area to get a

1 morphological characterization of the NGs by AFM. On Figure 3a, the confocal image and  
2 the associated fluorescence spectrum with a maximum at 576 nm exhibited the expected  
3 features for the HGdDOTA $\subset$ CS-Rhod/HA/TPP NGs, confirming the fact that the NGs are  
4 fluorescent. On Figure 3b, the same behavior was found for the HGdDOTA $\subset$ CS-  
5 Fluo/HA/TPP NGs with an emission at 511nm.

a-



b-

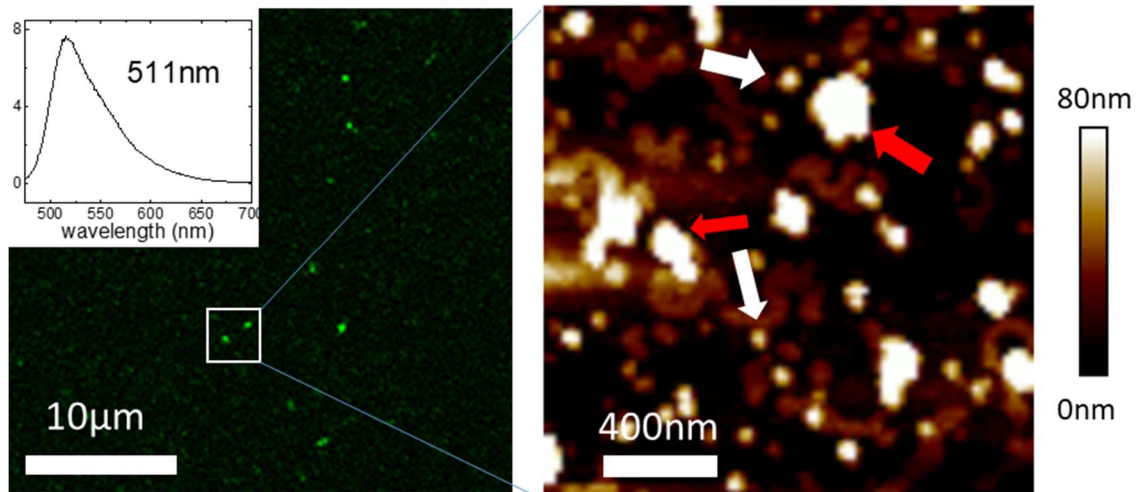


Figure 3: Confocal and associated AFM images of (a) HGdDOTA  $\subset$  CS-Rhod/HA/TPP NGs, and (b) HGdDOTA  $\subset$  CS-Fluo/HA/TPP NGs after dialysis.

6 Zooming with the AFM on a proper area allowed to show that, whatever the nanosuspensions,  
7 the NGs were spherical particles and no significant morphological differences could be  
8 noticed with a mix of isolated NPs (white arrows) or NG aggregates (red arrows). Whatever  
9 the samples (with, or without HGdDOTA), the isolated NG diameters calculated from the  
10 AFM images were inferior to 100 nm typically in the range of 60 nm (see Tables 1 and S5)

1 and the aggregates from 150 to 400 nm. Regarding the confocal images, the brighter and  
2 larger spots could be attributed to the aggregates. As for the comparison with the DLS  
3 measurements, such differences have already been observed for nanogels and could be  
4 attributed to the fact that in DLS, because of the presence of aggregates, the response could be  
5 biased by the use of mathematical models of signal processing (Rigaux et al., 2017).

6 Rhod and Fluo concentrations associated with nanogels were then determined by  
7 fluorescence. Rhod and Fluo concentrations associated with GdDOTA<sub>2</sub>-CS-Rhod-TPP/HA or  
8 GdDOTA<sub>2</sub>-CS-Fluo-TPP/HA NGs were 6.3 and 7.3 μM respectively. Furthermore, emission  
9 spectra of GdDOTA<sub>2</sub>-CS-Rhod-TPP/HA or GdDOTA<sub>2</sub>-CS-Fluo-TPP/HA nanosuspensions  
10 were superimposable to those of unloaded CS-Rhod-TPP/HA or CS-Fluo-TPP/HA nanogels  
11 (Figure S6), which showed that the presence of HGdDOTA within the nanoparticles did not  
12 perturb their fluorescent response. As shown above (Figure 3), confocal microscopy images  
13 of nanogels confirmed that all the CS-Rhod-TPP/HA or CS-Fluo-TPP/HA NGs were red and  
14 green emitters respectively.

15 Before testing the effectiveness of GdDOTA<sub>2</sub>-CS-Rhod-TPP/HA and GdDOTA<sub>2</sub>-CS-Fluo-  
16 TPP/HA NGs in enhancing the MRI signal, their potential cytotoxicity towards cells, was  
17 evaluated by means of MTT and LDH assays (Figure 4) (Fotakis & Timbrel 2006). For that, a  
18 murine macrophage cell line (RAW 264.7) was chosen, since macrophages are among the  
19 major cells mediating the inflammatory response to foreign substances, especially  
20 nanoparticles (Jiang et al. 2017). A20 cells which are lymphocyte cells were chosen as they  
21 are involved in the immune system (Gheran et al. 2017).

22

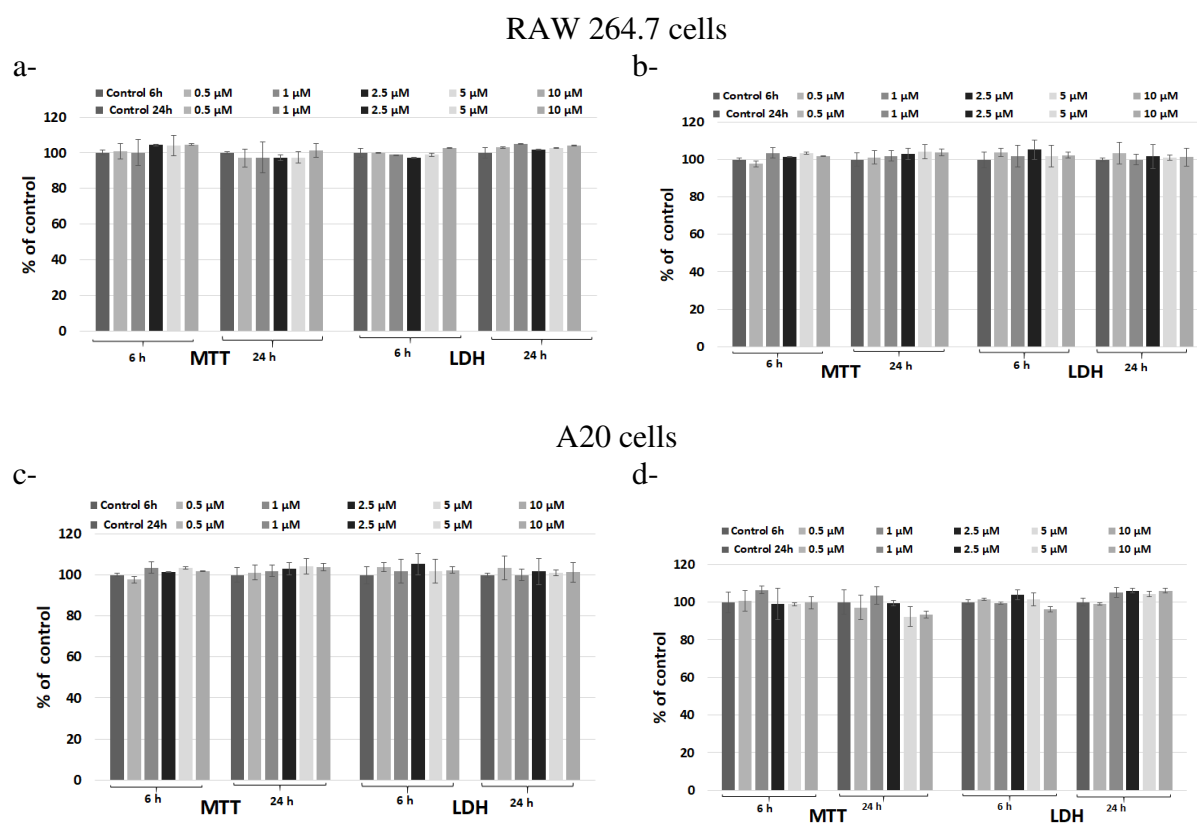


Figure 4: Cell viability and cytotoxicity established by MTT and LDH assays in the presence of RAW 264.7 cells and A20 cells after exposure to 0.5, 1, 2.5, 5 and 10  $\mu\text{M}$  Gd of a and c - GdDOTA<sub>C</sub>-CS-Rhod-TPP/HA and b and d- GdDOTA<sub>C</sub>-CS-Fluo-TPP/HA NGs for 6 and 24 hours. Results are calculated as means  $\pm$  sd ( $n = 3$ ) and expressed as % from controls (untreated cells).

- 1 The exposure of RAW264.7 and A20 cells to fluorescent Gd nanogels did not affect the cell
- 2 survival. Furthermore, this absence of toxicity is similar to the one observed for the non-
- 3 fluorescent analogues (Gheran et al. 2018, Gheran et al. 2017) which highlighted that
- 4 fluorophore grafting, while providing additional imaging functionality, did not affect the
- 5 harmlessness of nanogels to cells.
- 6 Finally, in order to evaluate the MRI efficiency of GdDOTA<sub>C</sub>-CS-Rhod-TPP/HA and
- 7 GdDOTA<sub>C</sub>-CS-Fluo-TPP/HA NGs, their longitudinal relaxation rates were recorded at 37°C,
- 8 as a function of resonance frequency. The corresponding NMR dispersion profiles (NMRD)
- 9 (Figure 5) revealed a maximum in relaxivity between 25 and 30 MHz
- 10 ( $r_1 \geq 80 \text{ mM}^{-1}\text{s}^{-1}$ ) by comparison to GdDOTA relaxivity in the same field region
- 11 ( $r_1 \sim 3.5 \text{ mM}^{-1}\text{s}^{-1}$  at 20 MHz) (Idée et al. 2006).

12

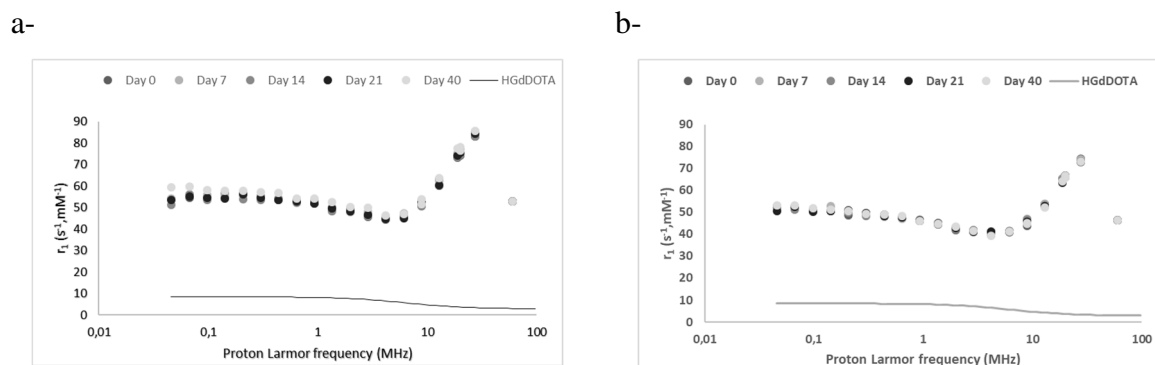


Figure 5: NMRD relaxivity profiles of a-  $GdDOTA \subset CS-Rhod-TPP/HA$  NGs and b-  $GdDOTA \subset CS-Fluo-TPP/HA$  NGs and their evolution over time (37°C)

1 These profiles shapes were typical of Gd chelate with a restricted rotational motion (Merbach,  
 2 Helm & Toth, 2013). Indeed, the spatial confinement of GdCAs within nanohydrogels  
 3 allowed to slow-down their tumbling motion. Furthermore, the hydrophilic nature of CS and  
 4 HA (Basu et al., 2015) that constituted the nanogel polymer matrix allowed the optimization  
 5 of water residence times in the gadolinium coordination sphere, leading to a strong outer-  
 6 sphere and/or second-sphere contribution to the relaxivity. Moreover, one should notice that  
 7 each profile shape was maintained over a period of 40 days (Figure 5), which demonstrated  
 8 the stability of  $GdDOTA \subset CS-Rhod-TPP/HA$  and  $GdDOTA \subset CS-Fluo-TPP/HA$  nanogels as  
 9 well as their ability to contain their Gd loading over the time.

10 In order to check how this relaxation amplification could be translated into magnified MR  
 11 images,  $T_1$ - and  $T_2$ -weighted images of phantoms containing  $GdDOTA \subset CS-Rhod-TPP/HA$   
 12 and  $GdDOTA \subset CS-Fluo-TPP/HA$  suspensions were acquired on a 3T clinical imager, with  
 13 DOTAREM® as control (Figure 6).

14

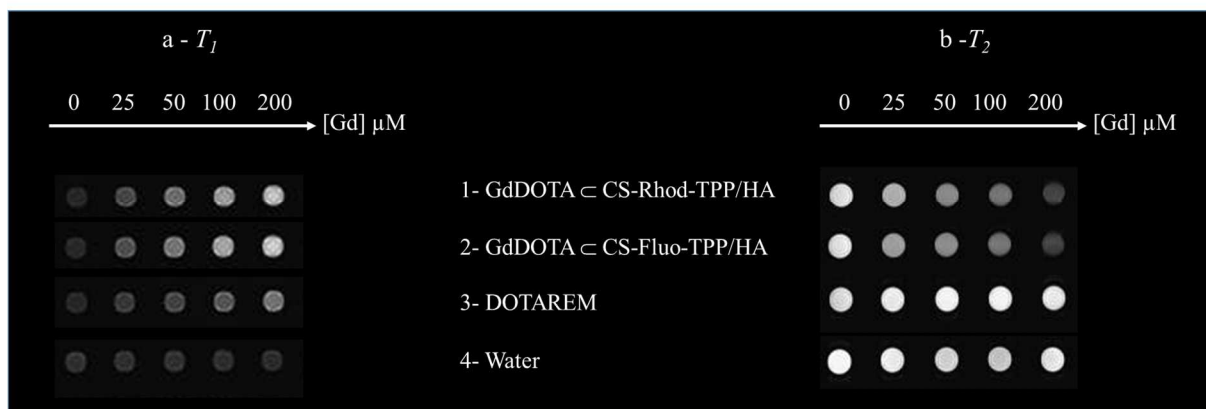


Figure 6: a)  $T_1$ - and b)  $T_2$ - weighted images of GdDOTA  $\subset$  CS-Rhod-TPP/HA (line 1) and GdDOTA $\subset$ CS-Fluo-TPP/HA NPs (line 2), DOTAREM® (line 3) and water (line 4) as controls. All samples were imaged at 3T, 37°C with 3D fast spin echo  $T_1$  or  $T_2$  sequences.

1 For the  $T_1$ -weighted images, the bright signal enhancement progressively increased with  
 2 increased gadolinium concentrations in nanogels. Comparison with DOTAREM® control  
 3 showed that the signal enhancement was due to the incorporation of GdDOTA within the  
 4 fluorescent CS-TPP/HA nanogels. Indeed, encapsulation of large amounts of GdDOTA in  
 5 nanogels resulted in an apparent increase in the mass of the complex and then in a restriction  
 6 of its rotational motion, which was responsible for the exaltation of the relaxivity (Merbach et  
 7 al. 2013). Conversely for the  $T_2$ -weighted images, under the same conditions, image  
 8 darkening was observed. This important  $T_2$  effect at high magnetic field results from the slow  
 9 rotation of the encapsulated complexes and/or magnetic susceptibility effects (Aime et al.,  
 10 2007). As a result, these images corroborated relaxometric measurements and confirmed the  
 11 dual  $T_1/T_2$  properties of the gadolinium loaded nanogels.

12

## 13 2. Conclusion

14 In this paper, we reported the synthesis and the characterization of a series of fluorescent  
 15 chitosans and the subsequent synthesis of biocompatible nanohydrogels by ionic gelation in  
 16 the presence of hyaluronic acid. MRI and optical imaging modalities were set within the  
 17 nanogels thanks to chitosan and encapsulation of Gd chelate during the process. The low  
 18 degree of substitution of chitosans by fluorophores and the hypersensitive MRI character of  
 19 Gd chelate buried within the nanoparticles allowed to take into account the differences in  
 20 sensibility between MRI and optical imaging modalities, so as to obtain an optimal signal in  
 21 both modalities. Both MRI and optical imaging activities were evaluated.  $T_1$  and  $T_2$ -weighted

1 phantom MR images of nanogels, recorded on a 3T clinical scanner, showed an increase in  
2 image contrast for lesser Gd doses, by comparison to those used with DOTAREM<sup>®</sup>. The huge  
3 content of water and the presence of Gd chelate within the nanogels did not seem to quench  
4 their emission. This absence of quenching was demonstrated in fluorescence imaging by their  
5 red or green emission. Further work is in progress in order to produce CS-TPP/HA  
6 nanohydrogels able to combine multicolor optical coding for multiplexing and magnetic  
7 properties.

8

## 9 **ACKNOWLEDGEMENTS**

10 Yarong Shi (Bruker Nano, Inc, Santa Barbara, CA 93117, USA and LRN EA4682,  
11 University of Reims Champagne Ardenne), Christine Terryn (PICT platform, University of  
12 Reims Champagne-Ardenne) and Christophe Portefaix (Radiology Department, CHU de  
13 Reims – Hôpital Maison Blanche) are gratefully acknowledged for their help in AFM  
14 measurements, optical imaging and MRI experiments respectively.

15 The authors would like to thank the “Programme de coopération transfrontalière Interreg  
16 France-Wallonie-Vlaanderen” for funding the “Nanocardio” project (<http://nanocardio.eu>) and  
17 the post-doctoral fellowship of V. Malyskyi, the PHC Brancusi program (project n°  
18 43465WA) and the PIAnET platform (supported by the European Regional Development  
19 Fund and the Region Champagne Ardenne). This work was also performed with the financial  
20 support of the FNRS, FEDER, the ARC, the Walloon Region (Biowin and Interreg projects)  
21 and the COST actions. Authors thank the Center for Microscopy and Molecular Imaging  
22 (CMMI, supported by European Regional Development Fund Wallonia) and the Bioprofiling  
23 platform (supported by the European Regional Development Fund and the Walloon Region,  
24 Belgium). Finally, this work was supported by a grant of the Romanian Ministry of Research  
25 and Innovation, CCCDI-UEFISCDI, project number PN III-P3-3.1-PM-RO-FR-2019-  
26 0204/6BM/2019, within PNCDI III.

27

## 28 **REFERENCES**

29 Aime, S., Delli Castelli, D., Lawson, D.& Terreno, E. (2007) Gd-loaded liposomes as T1,  
30 susceptibility, and CEST agents, All in One. *J. Am. Chem. Soc.*, 129 (9), 2430-2431.  
31 Asberg, P., Nilsson, P.& Inganas, O. Fluorescence quenching and excitation transfer between  
32 semiconducting and metallic organic layers. *J. Appl. Phys.*, 96 (6), 3140.

1 Augé, S., Amblard-Blondel, B. & Delsuc, M. A. (1999). Investigation of the diffusion  
2 measurement using PFG and tTest r against experimental conditions and parameters. *J. Chim.*  
3 *Phys. Phys.-Chim. Biol.*, 96(9–10), 1559–1565.

4 Basu, A., Kunduru, K. R., Abtew, E. R. & Domb, R. T. (2015). Polysaccharide-Based  
5 Conjugates for Biomedical Applications. *Bioconjugate Chem*, 26(8), 1396 – 1412.

6 Belabassi, Y., Moreau, J., Gheran, V., Henoumont, C., Robert, A., Callewaert, M., Rigaux,  
7 G., Cadiou, C., Vander Elst, L., Laurent, S., Muller, R. N., Dinischiotu, A., Voicu, S. N. &  
8 Chuburu, F. (2017). Synthesis and characterization of PEGylated and fluorinated chitosans:  
9 application to the synthesis of targeted nanoparticles for drug delivery. *Biomacromolecules*,  
10 18(9), 2756–2766.

11 Berger, J., Reist, M., Mayer, J. M., Felt, O., Peppas, N. A. & Gurny, R. (2004). Structure and  
12 interactions in covalently and ionically crosslinked chitosan hydrogels for biomedical  
13 applications. *Eur. J. Pharm. Biopharm.*, 57, 19-34.

14 Callewaert, M., Roullin, V. G., Cadiou, C., Millart, E., Van Gulik, L., Andry, M. C.,  
15 Portefaix, C., Hoeffel, C., Laurent, S., Vander Elst, L., Muller, R., Molinari, M., & Chuburu,  
16 F. (2014). Tuning the composition of biocompatible Gd nanohydrogels to achieve  
17 hypersensitive dual T1/T2 MRI contrast agents. *J. Mater. Chem. B*, 2 (37), 6397–6405.

18 Courant, T., Roullin, V. G., Cadiou, C., Callewaert, M., Andry, M. C., Portefaix, C., Hoeffel,  
19 C., de Goltstein, M. C., Port, M., Laurent, S., Vander Elst, L., Muller, R., Molinari, M., &  
20 Chuburu, F. (2012). Hydrogels Incorporating GdDOTA: Towards Highly Efficient Dual  
21 T1/T2 MRI Contrast Agents. *Angew. Chem., Int. Ed. Engl.*, 51(36), 9119–9122.

22 Fotakis, G. & Timbrell, J. A. (2006). In vitro cytotoxicity assays: Comparison of LDH,  
23 neutral red, MTT and protein assay in hepatoma cell lines following exposure to cadmium  
24 chloride. *Toxicol. Lett.*, 160, 171–177.

25 Gheran, C.V., Voicu, S.N., Rigaux, G., Callewaert, M., Chuburu, F., & Dinischiotu, A.  
26 (2017). Biological effects induced by Gadolinium nanoparticles on Lymphocyte A20 cell line.  
27 *The EuroBiotech Journal*, 1, 57–64.

28 Gheran, C. V., Rigaux, G., Callewaert, M., Berquand, A., Molinari, M., Chuburu, F., Voicu,  
29 S. N., & Dinischiotu, A. (2018). Biocompatibility of Gd-Loaded Chitosan-Hyaluronic Acid  
30 Nanogels as Contrast Agents for Magnetic Resonance Cancer Imaging. *Nanomaterials*, 8(4),  
31 201.

32 Gianolio, E., Bardini, P. Arena, F., Stefania, R. Di Gregorio, E., Iani, R. & Aime, S. (2017).  
33 Gadolinium retention in the rat brain: assessment of the amounts of insoluble gadolinium-

1 containing species and intact gadolinium complexes after repeated administration of  
2 gadolinium-based contrast agents. *Radiology*, 285(3), 839–849.

3 Gupta, A., Caravan, P., Price, W. S., Platas-Iglesias, C., & Gale, E. M. (2020). Applications  
4 for transition-metal chemistry in contrast-enhanced magnetic resonance imaging. *Inorg.*  
5 *Chem.*, 59, 6648-6678.

6 Gupta, K. C. & Jabrail, F.H. (2006). Preparation and characterization of sodium hexameta  
7 phosphate cross-linked chitosan microspheres for controlled and sustained delivery of  
8 centchroman. *Int. J. Biol. Macromol.*, 38, 272-283.

9 Hirai, A., Odani, H., & Nakajima, A (1991). Determination of Degree of Deacetylation of  
10 Chitosan by H NMR Spectroscopy. *Polymer. Bulletin*, 26(1), 87–94.

11 Idée, J. M., Port, M., Raynal, I., Schaefer, M., Le Greneur, S. & Corot, C. (2006).  
12 *Fundamental & Clinical Pharmacology*, 20, 563-576.

13 Johnson, C. S, Jr. (1999). Diffusion Ordered Nuclear Magnetic Resonance Spectroscopy:  
14 Principles and Applications. *Prog. Nucl. Magn. Reson. Spectrosc*, 34(3–4), 203–256.

15 Jiang, L.Q., Wang, T.Y., Webster, T.J., Duan, H.J., Qiu, J.Y., Zhao, Z.M., & Zheng, C.L.  
16 (2017). Intracellular disposition of chitosan nanoparticles in macrophages: intracellular  
17 uptake, exocytosis, and intercellular transport. *Int. J. Nanomed.*, 12, 6383-6388.

18 Kanda, T., Oba, H., Toyoda, K., Kitajima, K., & Furui, S. (2016). Brain gadolinium  
19 deposition after administration of gadolinium-based contrast agents. *Jpn. J. Radiol.*, 34, 3-9.

20 Khawaja, A. Z., Cassidy, D. B., Al Shakarchi, J., McGrogan, D. G., Inston, N. G., & Jones, R.  
21 G. (2015). Revisiting the risks of MRI with Gadolinium based contrast agents—review of  
22 literature and guidelines. *Insights Imaging*, 6, 553–558.

23 Leng, T., Jakubek, Z. J., Mazloumi, M., Leung, A. C. W., & Johnston, L. J. (2017). Ensemble  
24 and Single Particle Fluorescence Characterization of Dye-Labeled Cellulose Nanocrystals.  
25 *Langmuir*, 33(32), 8002–8011.

26 Lux, J., Chan, M., Van der Elst, L., Schopf, E., Mahmoudi, S., Laurent, S., & Almutairi A.  
27 (2013). Metal chelating crosslinkers form nanogels with high chelation stability. *J. Mater.*  
28 *Chem. B*, 1, 6359-6354.

29 Ma, O., Lavertu, M., Sun, J., Nguyen, S., Buschmann, M. D., Winni, F. M., & Hoemann, C.  
30 D. (2008). Precise derivatization of structurally distinct chitosans with rhodamine B  
31 isothiocyanate. *Carbohydr. Polym.*, 72(4), 616–624.

32 Mei, S., Zhou, J., Sun, H-T., Cai, Y., Sun, L-D., Jun, D.& Yan, C-H. (2021). Networking state  
33 of ytterbium ions probing the origin of luminescence quenching and activation in  
34 nanocrystals. *Adv. Sci.*, 8(6), 2003325.

1 Merbach, A. E., Helm, L., & Toth, E. (2013). *The Chemistry of Contrast Agents in Medical*  
2 *Magnetic Resonance Imaging* (2<sup>nd</sup> Ed.) Chichester: Wiley and Sons).

3 Rigaux, G., Gheran, C. V., Callewaert, M., Cadiou, C., Voicu, S. N., Dinischiotu, A., Andry,  
4 M. C., Vander Elst, L., Laurent, S., Muller, R. N., Berquand, A., Molinari, M., Huclier-  
5 Markai, S., & Chuburu, F. (2017). A multi-technique approach combining DLS, AF4 and  
6 AFM in liquid mode to select Gd-loaded chitosan-TPP nanohydrogels for MRI positive  
7 contrast agent for Lymph Node Imaging. *Nanotechnology*, 28, Article ID 055705.

8 Rogosnitzky, M. & Branch, S. (2016). Gadolinium-based contrast agent toxicity: a review  
9 of known and proposed mechanisms. *Biometals*, 29 (3) 365–376.

10 Sang, Z., Quan, J., Han, J., Deng, X., Shen, J., Li, G. & Xie, Y. (2020). Comparison of three  
11 water-soluble polyphosphate tripolyphosphate, phytic acid, and sodium hexametaphosphate as  
12 crosslinking agents in chitosan nanoparticle formulation. *Carbohydrate Polymers*, 230,  
13 115577.

14 Sinagaglia, G., Magro, M., Miotto, G., Cardillo, S., Agostinelli, E., Zboril, R., Bidollari, E., &  
15 Vianello, F. (2012). Catalytically active bovine serum amine oxidase bound to fluorescent and  
16 magnetically drivable nanoparticles. *Int. J. Nanomed.*, 7, 2249–2259.

17 Soleimani, A., Martinez, F., Economopoulos, V., Foster, P. J., Scholl, T. J., & Gillies, E. R.  
18 (2013). Polymer cross-linking: a nanogel approach to enhancing the relaxivity of MRI  
19 contrast agents. *J. Mater. Chem. B.*, 1, 1027-1034.

20 Vårum, K. M., Antohonsen, M. W., Grasdalen, H., & Smidsrød, O (1991). Determination of  
21 the Degree of N-Acetylation and the Distribution of N-Acetyl Groups in Partially N-  
22 Deacetylated Chitins (Chitosans) by High-Field NMR Spectroscopy. *Carbohydr. Res.*, 211,  
23 17–23.

24 Washner, J., Gael, E. M., Rodriguez-Rodriguez, A., & Caravan, P. (2019). Chemistry of MRI  
25 contrast agents: current challenges and new frontiers. *Chem. Rev.*, 119, 957-1057.

26 Xia, S., Yang, H., Duan, L., Gao, G. H., & Zhang, X. (2016). A potential dual-modality optical  
27 imaging probe based on the pH-responsive micelle. *J. Polym. Res.*, 23, 179.

28

Graphical abstract

